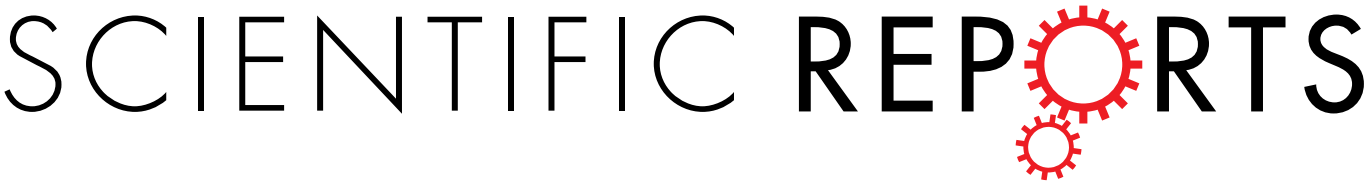

OPEN

Charge Berezinskii-Kosterlitz-Thouless transition in superconducting NbTiN films

Received: 4 January 2018
Accepted: 22 February 2018
Published online: 06 March 2018

Alexey Yu. Mironov[1,2], Daniel M. Silevitch[4], Thomas Proslier[5], Svetlana V. Postolova[1,2], Maria V. Burdastyh[1,2], Anton K. Gutakovskii[1,2], Thomas F. Rosenbaum[4], Valerii V. Vinokur[6,7] & Tatyana I. Baturina[1,2,3,8]

Three decades after the prediction of charge-vortex duality in the critical vicinity of the two-dimensional superconductor-insulator transition (SIT), one of the fundamental implications of this duality—the charge Berezinskii-Kosterlitz-Thouless (BKT) transition that should occur on the insulating side of the SIT—has remained unobserved. The dual picture of the process points to the existence of a superinsulating state endowed with zero conductance at finite temperature. Here, we report the observation of the charge BKT transition on the insulating side of the SIT in 10 nm thick NbTiN films, identified by the BKT critical behavior of the temperature and magnetic field dependent resistance, and map out the magnetic-field dependence of the critical temperature of the charge BKT transition. Finally, we ascertain the effects of the finite electrostatic screening length and its divergence at the magnetic field-tuned approach to the superconductor-insulator transition.

In the early 1970s, Vadim Berezinskii[1], Michael Kosterlitz, and David Thouless[2,3] introduced the idea of a topological phase transition in which pairs of bound vortex excitations unbind at a critical temperature T_{BKT}. The nature of the Berezinskii-Kosterlitz-Thouless (BKT) transition is different from the standard phase transitions described by the Landau paradigm. There is no symmetry breaking associated with the onset of the order parameter, but instead there is a change in the behavior of the two-point correlation function. At $T < T_{BKT}$ it decays algebraically, changing to exponential for $T > T_{BKT}$. Thin superconducting films soon became the principal experimental realization for studying the BKT transition[4,5]. However, detailed investigations of the physics of the superconductor-insulator transition (SIT) in Josephson junction arrays (JJA) led to the prediction that the charge-anticharge unbinding BKT transition should appear at finite temperature on the insulating side of the SIT[6–8]. Using the framework of gauge theory, Diamantini *et al.*[9] demonstrated that in the planar JJA, the vortex-charge duality leads to a zero-temperature quantum phase transition between a superconductor and its mirror image, a state with zero conductance, which they termed a superinsulator. The physical origin of a superinsulating state is the charge confinement due to the logarithmic interaction between the charges in two-dimensional (2D) systems[6,10,11]. In disordered superconducting films, the charge confinement on the insulating side of the SIT results from the divergence of the dielectric constant ε in the critical vicinity of the transition. The logarithmic interaction holds over distances $d < r \lesssim \Lambda \simeq \varepsilon d$, where d is the thickness of the film and Λ is the electrostatic screening length[11]. This parallels the logarithmic interaction between vortices on the superconducting side, which causes the vortex binding-unbinding topological BKT transition into the superconducting state at finite temperature $T = T_{VBKT}$[1–3]. Accordingly, logarithmic interactions between charges on the insulating side of the SIT is expected to give rise to a classical charge BKT transition into the superinsulating state with the

[1]A. V. Rzhanov Institute of Semiconductor Physics SB RAS, 13 Lavrentjev Avenue, Novosibirsk, 630090, Russia. [2]Novosibirsk State University, Pirogova str. 2, Novosibirsk, 630090, Russia. [3]The James Franck Institute and Department of Physics, The University of Chicago, Chicago, IL, 60637, USA. [4]Division of Physics, Mathematics, and Astronomy, California Institute of Technology, Pasadena, CA, 91125, USA. [5]Institut de recherches sur les lois fundamentales de l'univers, Commissariat de l'énergie atomique et aux énergies renouvelables-Saclay, Gif-sur-Yvette, France. [6]Materials Science Division, Argonne National Laboratory, 9700 S. Cass Ave, Argonne, IL, 60439, USA. [7]Computation Institute, University of Chicago, 5735 S. Ellis Avenue, Chicago, IL, 60637, USA. [8]Departamento de Física de la Materia Condensada, Instituto de Ciencia de Materiales Nicolás Cabrera and Condensed Matter Physics Center (IFIMAC), Universidad Autónoma de Madrid, 28049, Madrid, Spain. Correspondence and requests for materials should be addressed to V.V.V. (email: vinokour@anl.gov)

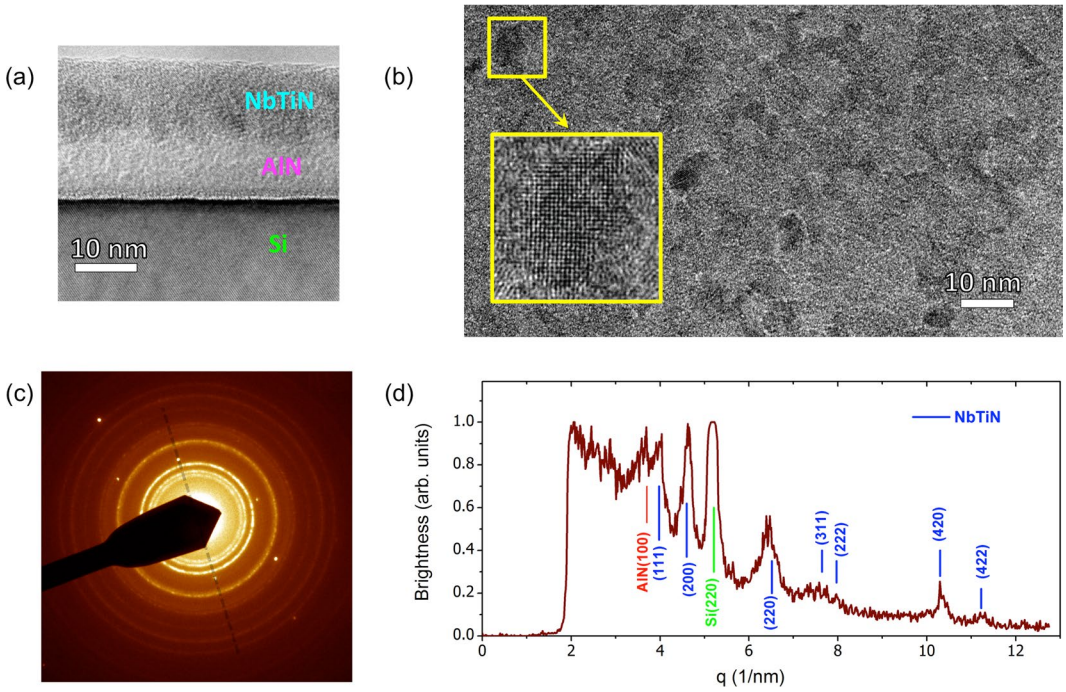

Figure 1. Structure and composition of a 10 nm thick NbTiN film. (**a**) Cross-section of the film from High Resolution Transmission Electron Microscopy (HRTEM). (**b**) HRTEM plan view bright field image. The yellow square shows a magnified image of one of the crystallites. (**b**) Electron-diffraction data of the film. The rings are characteristic of polycrystalline structures; the bright spots arise from the crystalline lattice of the underlying Si substrate. (**d**) Electron diffraction data from the panel (c) taken along the self-transparent dashed line in panel (c) and plotted as the intensity vs. the wavenumber. Several Bragg peaks from the NbTiN film are observed, along with the (220) peak from the Si substrate and the (100) peak from the AlN buffer layer.

conductance going to zero at a finite temperature $T = T_{CBKT}$[10–12]. Applied magnetic fields can tune the SIT with high resolution, offering a window into unexplored electronic functionalities. In the critical vicinity of the SIT on the superconducting side the system should possess superinductance[13], and at the insulating side the system is expected to be a supercapacitor due to a diverging dielectric constant[11]. This calls for a thorough study of the highly resistive state that terminates two-dimensional superconductivity at the quantum critical point whose nature remains a subject of intense research[10,14–19].

Existing experimental data on JJA[20–22], superconducting wire networks[23], InO_x[19], andTiN films[18,24] support the picture of the dual vortex-charge BKT transitions and corresponding formation of the mirror superconducting-superinsulating states. While there have been numerous experimental hallmarks of superinsulating behavior, the evidence for the charge BKT transition, with its characteristic criticality (see Eq. (1) below), has remained elusive. To address this challenge, we examine a NbTiN film, which is expected to combine the high stability of TiN films with the enhanced superconducting transition temperature T_c of NbN films, due to a larger Cooper pairing coupling constant as compared to TiN. We thus expect that T_{CBKT} is likewise enhanced, opening a wider window for observing critical behavior.

Sample preparation

To grow suitable NbTiN films, we employed the atomic layer deposition (ALD) technique based on sequential surface reaction step-by-step film growth. The fabrication technique is described in detail in the Supplemental Material. This highly controllable process provides superior thickness and stoichiometric uniformity and an atomically smooth surface[25,26] as compared to chemical vapor deposition, the standard technique used to grow NbTiN films[27]. We used $NbCl_5$, $TiCl_4$, and NH_3 as gaseous reactants; the stoichiometry was tuned by varying the ratio of $TiCl_4/NbCl_5$ cycles during growth[28]. The superconducting properties of these ultrathin NbTiN films were optimized by utilizing AlN buffer layers grown on top of the Si substrate[29]. NbTiN films of thicknesses $d = 10$, 15, and 20 nm were grown, varying only the number of ALD cycles (240, 420, and 768 cycles, respectively), with all other parameters of the ALD process held constant. We show in Fig. 1(a) a high-resolution transmission electron microscopy (HRTEM) image of the cross-section of the 10 nm thick NbTiN film. It reveals that both the AlN buffer layer and the NbTiN have a fine-dispersed polycrystalline structure. Presented in Fig. 1(b) is a plan view of a large area containing many crystallites. The densely packed crystallites have different orientations and are separated by atomically thin inter-crystallite boundaries. A statistical analysis of the image finds the average crystallite size to be approximately 5 nm. The electron diffraction data for the film are shown in Fig. 1(c). The clearly seen rings confirm a polycrystalline structure. The analysis of the diffraction data along the direction [220] of the Si substrate displayed in Fig. 1(d) reveals that the NbTiN crystallites have the same rock-salt crystal structure as both NbN and TiN. Using Vegard's law, we find that our NbTiN film is an approximately 7:3 solid solution of NbN

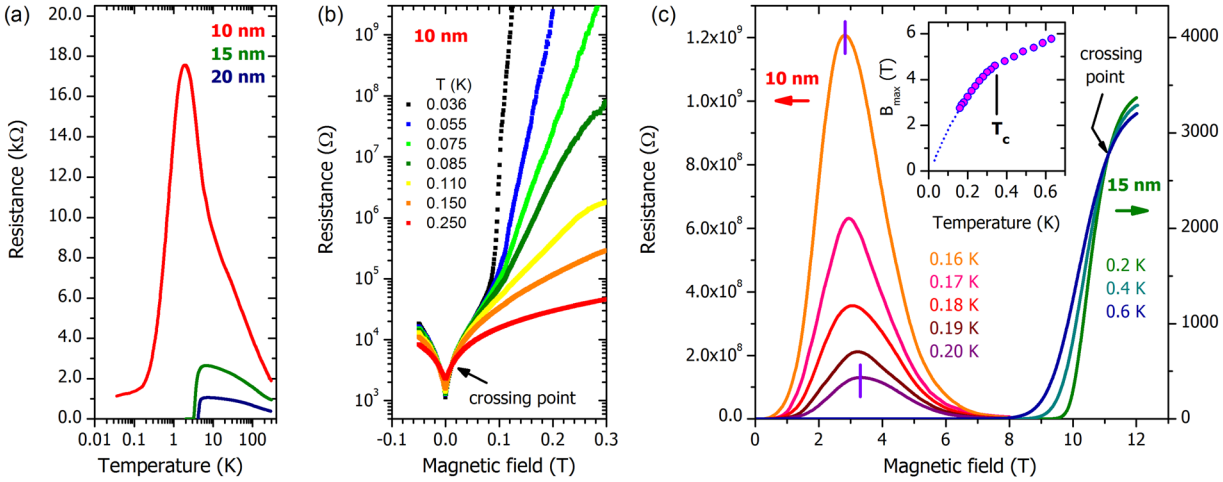

Figure 2. Temperature and magnetic field dependences of the resistance of NbTiN films. (**a**) The temperature dependences of the resistance in zero magnetic field for three NbTiN films of thicknesses 10, 15, and 20 nm, respectively. (**b**) Low-field isothermal magnetoresistance of the 10 nm thick film at different temperatures. At temperatures below 0.1 K, the magnetoresistance develops a sharp kink for $B < 0.1$ T, moving to lower magnetic fields as the temperature is further lowered. Above the kink, even a small increase in the field results in a sharp increase of the resistance by several orders of magnitude. The crossing point, $R_c = 4.7\,\mathrm{k\Omega}$, $B_{SIT} = 0.015$ T, separates the regions with $dR/dT < 0$ and $dR/dT > 0$. (**c**) Magnetoresistance of the 10 nm and 15 nm thick films on a linear field scale. The left ordinate corresponds to the data for 10 nm thick film taken in the 0.16–0.20 K temperature range, and the right hand ordinate refers to the data in the 0.2 – 0.6 K interval for the 15 nm thick film. Note that the two resistance scales differ by a factor of $3 \cdot 10^5$. The magnetoresistance of the 15 nm thick film exhibits the conventional superconducting behavior with a well-defined upper critical field $B_{c2}(0) = 10.5$ T and the crossing point at $B_c = 11$ T stemming from the interplay of superconducting fluctuations contributing to conductivity[41,42], and similar to behavior observed in materials such as InO_x[43]. By contrast, the magnetoresistance of the 10 nm thick film develops a colossal insulating peak at fields well below B_{c2}. The vertical strokes on the 0.16 K and 0.20 K curves for the 10 nm thick film mark the fields B_{max} at which the magnetoresistance peaks are achieved. The inset presents the temperature dependence of B_{max} (symbols). The dotted line, extrapolating the data to the $T \to 0$ limit, illustrates the trend of B_{max} of shifting towards almost zero field upon decreasing temperature.

and TiN (See Supplemental Material for further information on the fabrication and measurement techniques, films structural, superconducting and transport parameters, and I–V characteristics).

The films were lithographically patterned into bars and resistivity measurements were performed at sub-Kelvin temperatures in helium dilution refrigerators (see the details of the sample geometry and measurement technique in (See Supplemental Material for further information on the fabrication and measurement techniques, films structural, superconducting and transport parameters, and I–V characteristics)). The temperature dependences of the resistance, $R(T)$, given as resistance per square, are shown in Fig. 2(a) over four decades in temperature. Upon cooling in zero magnetic field, all three films undergo a superconducting transition that manifests as a severe resistance drop. The superconducting transition temperature, T_c, is determined by the inflection point of $R(T)$ and marks the temperature at which thermodynamically stable Cooper pairs appear. For the most highly disordered sample, this precedes the point at which global phase coherence, and hence zero resistivity, occurs[30]. Instead, with decreasing film thickness (and increasing disorder), spatial fluctuations of the superconducting gap become increasingly important, giving rise to the formation of self-organized structures of superconducting islands in a non-superconducting environment[31,32]. The temperature T_c decreases with decreasing film thickness and consequent increasing sheet resistance.

Results

The resistances of all three films exhibit peaks at temperatures just above T_c, with the peak amplitudes increasing as the thickness decreases. Similar trends were observed in the parent compounds TiN[33] and NbN[34] near the SIT and were attributed to quantum contributions to conductivity due to weak localization and electron-electron interaction effects. The sheet resistance of the thinnest film achieves a maximum of 17.56 kΩ/□; notably, this well exceeds the quantum resistance $R_Q = h/(2e)^2 = 6.45\,\mathrm{k\Omega}/\square$ which was widely believed to be the upper boundary for the existence of superconductivity in two dimensions[35–37]. A similar peak of 29.4 kΩ/□, well above R_Q, was seen in TiN[38].

Focusing on the behavior of the thinnest film ($d = 10$ nm), where the degree of disorder permits fully tuning the sample with experimentally-accessible magnetic fields, we note first that the global coherent superconducting state is not achieved at lowest temperatures. Instead, the behavior of the zero field resistivity suggests that the film falls into the Bose metallic state[39], featuring a finite density of free vortices. The appearance of such vortices in the absence of a magnetic field is a fundamental feature of the BKT transition, which revolves around thermal

fluctuations inducing vortex-antivortex pairs. Figure 2(b) presents a set of magnetoresistance curves, $R(B)$, taken at different temperatures below $T_c = 0.33$ K determined by the inflection point of $R(T)$ at zero magnetic field. All of the $R(B)$ data presented below were measured at voltages $V = 100\ \mu$V, i.e. in the low-voltage response regime (see the discussion in the end of the "Data analysis" section below). Prominent features of these magnetoresistance curves, especially profound at lowest temperatures, are the crossing point at very low field $B_{SIT} = 0.015$ T that marks the SIT (discussed below) and the sharp kink at some temperature-dependent magnetic field above which the resistance increases extremely quickly as a function of field. The field associated with the kink shifts to lower fields with decreasing temperature. Inspecting the magnetoresistance behavior in the large field interval, one sees that it shows inherently non-monotonic behavior marked by a colossal insulating peak, see Fig. 2(c). Importantly, these peaks develop at magnetic fields for which the thicker films are still fully superconducting, i.e. the field B_{max}, where the maximum is observed, is well below the upper critical field B_{c2}. This suggests that the indefinite growth of $R(B)$ at low temperatures/magnetic fields, as well as the peak in the resistance at higher temperatures in the 10 nm film, is an implication of Cooper pairing. The inset in Fig. 2(c) shows that the position of the maximum of the resistance peaks moves to lower fields with decreasing temperature. There is a kink in the $B_{max}(T)$ dependence at $T \simeq T_c$, with the slope decreasing significantly when passing to $T > T_c$. Extrapolating the data to $T \to 0$ shows that $B_{max}(T)$ shifts to nearly zero field upon decreasing the temperature. Taken together, this indicates that the mechanism that drives the system into the strongly localized state overpowers the effect of the suppression of the Cooper pairing by the magnetic field, which would be expected to diminish the resistance of the Cooper pair insulator[40]. Note here that the mere non-monotonicity of magnetoresistance cannot be taken as an indication of the SIT. For example, vortices crossing the superconducting wires under the applied current may also lead to large amplitude oscillations of the magnetoresistance.

To gain insight into the nature of the magnetic-field-induced states, we examine $R(T)$ at different magnetic fields. Figure 3(a) displays for the 10 nm thick film the fan-like set of magnetoresistance curves, characteristic of the magnetic field-induced SIT. The crossing point (B_{SIT}, R_c) in Fig. 2(b) now corresponds to nearly temperature independent $R(T)$ at $B = 0.015$ T, separating the superconducting and insulating behavior. Two important comments are in order here. First, the field of the crossing point $B_{SIT} = 0.015$ T is *two orders of magnitude lower* than the upper critical field B_{c2}. This distinguishes it from the crossing point displayed by the thicker film ($d = 15$ nm) occurring at 11 T and resulting from the quantum contributions to conductivity from superconducting fluctuations[41,42] as well as similar crossing points in materials such as InO_x[43]. Second, the resistance at the SIT is $R_c = 4.7\ \text{k}\Omega$, close but not equal to the quantum resistance $6.45\ \text{k}\Omega$.

Re-plotting these data as log R vs. $1/T$ curves in Fig. 3(b), we see that the behavior of the resistance in the entire temperature range cannot be reduced to the Arrhenius temperature dependence with a single activation energy. Qualitatively similar behavior has been observed in thin films of the parent compound TiN[18], as well as InO_x films[19] and patterned Josephson Junction Arrays[20]. Instead of simple Arrhenius behavior, there is a complicated evolution of the resistance curves with increasing magnetic field. While at low fields the $\log R(1/T)$ dependence exhibits hyperactivation, i.e. faster than thermally activated growth[18], at larger fields, the $\log R(1/T)$ curves exhibit a kink and bend down with decreasing temperature. We contrast this to the behavior of InO_x thin films[19], where hyperactivation was likewise observed, but is consistent with an Efros-Shklovskii model followed by a crossover to a Mott hopping regime[44]. As shown in Fig. 3(c), the NbTiN film exhibits a pronounced departure from Efros-Shklovskii behavior for $B \leq 8$ T.

In order to illuminate the physics governing the $R(T)$ behavior, we replot the low-field data as the conductances, $G = 1/R$, vs. temperature in Fig. 3(d). We see in the conductance curves an insulating analogue of the drop to zero of the resistance at the onset of superconductivity. In the dual mirror picture of the conductance, we thus see the transition of the system into a superinsulating state characterized by zero conductance at finite temperature. This suggests that we can write the conductance in the generic form $\ln G \propto -a/(T - T^*)^\alpha$ for the finite temperature zero conducting state. Using T^* as an adjusting parameter, we find that $\alpha = 0.48 \pm 0.03$ gives the best fit to the experimental data. This is consistent with $\alpha = 1/2$ corresponding to critical BKT behavior obtained by a detailed renormalization group analysis[45] of the system with infinite screening length:

$$G \propto \exp\left(-\frac{b}{\sqrt{(T/T_{CBKT}) - 1}}\right), \tag{1}$$

where T_{CBKT} replaces T^*, and b is a constant of order unity. In Fig. 3(e) we plot G vs. $(T/T_{CBKT} - 1)^{-1/2}$ for fields 0.12 and 0.25 T. The correct choice of the only adjustable parameter, T_{CBKT}, for each field (shown in the legend for Fig. 3(d)), produces a linear dependence, allowing the determination of b as the slope of the respective lines. The dashed lines in Fig. 3(d) correspond to Eq. (1). A close inspection of the fits reveals that while the conductance curves at $B = 0.12$ and 0.25 T precisely follow the formula over six decades, the 0.50 T curve displays a slight departure (Fig. 3(d)), indicating that the assumption of critical CBKT behavior combined with an infinite screening length has started to break down.

These results establish a superinsulator as a confined low temperature charge BKT phase of the Cooper pair insulator. In this phase, vortices form a Bose condensate that completely blocks the motion of the Cooper pairs.

Data analysis

To proceed further with the analysis, we choose the value of T_{CBKT} for every isomagnetic $G(T)$ curve and plot in Fig. 4(a) the conductance normalized by its value at temperature $T = 4T_{CBKT}$ vs. the normalized temperature $T/T_{CBKT}(B)$. The corresponding field-dependent charge BKT transition temperature T_{CBKT} is shown in Fig. 4(b). Remarkably, the complex diversity of the R(T) curves (exhibiting sub-activation at high magnetic field and hyper-activation at small field in Fig. 3(b)) rescaled onto a set of uniform curves that collapse at $T/T_{CBKT} > 2.5$. Moreover, the field-dependent evolution of the curve shapes, including the change in concavity, now reduces

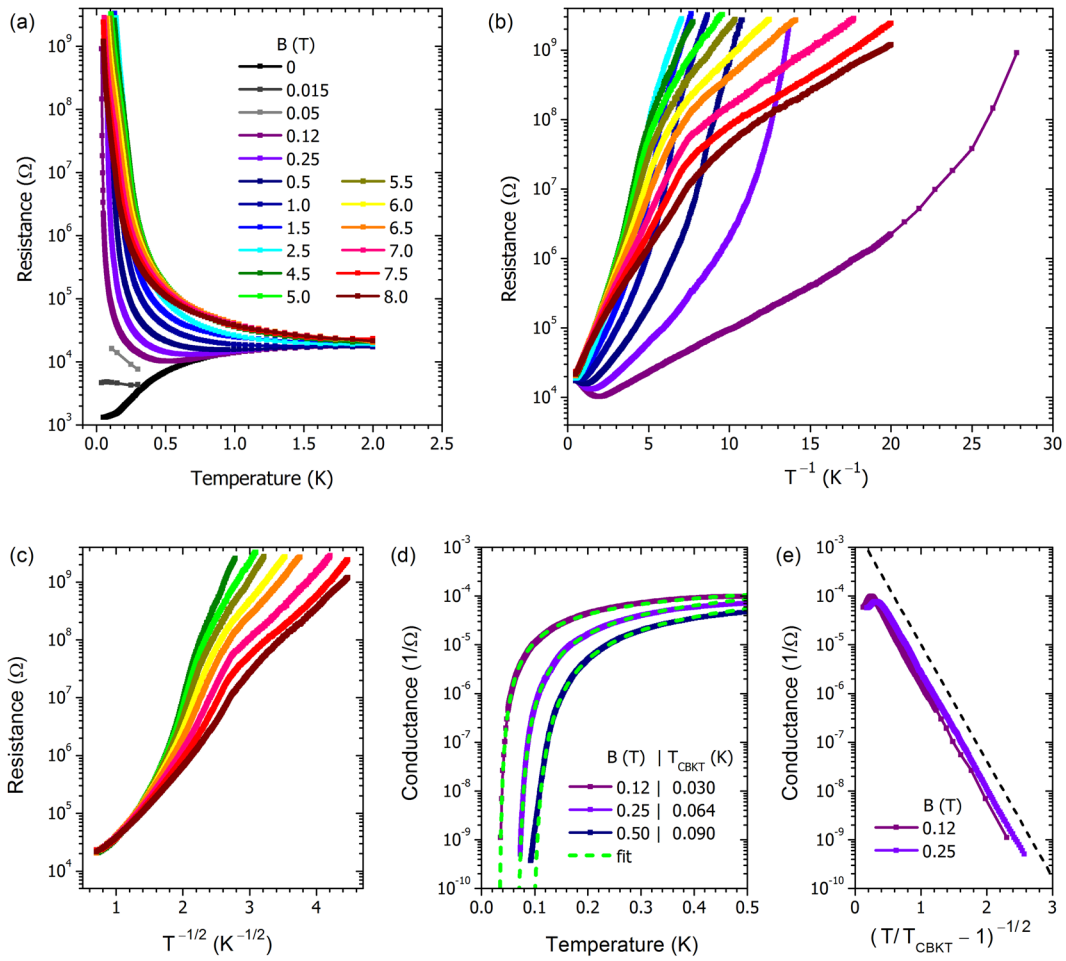

Figure 3. Temperature evolution of the magnetic field-induced states in the 10 nm thick NbTiN film. (**a**) Resistance vs. temperature at a series of magnetic fields listed in the legend in the panel (legend is the same for all the panels of this figure). (**b**) Resistance vs. inverse temperature at different magnetic fields. None of the temperature dependences can be modeled as Arrhenius behavior with a single activation energy. (**c**) Resistance vs. $T^{-1/2}$ for magnetic fields between 4.5 and 8 T. Efros-Shklovskii behavior is likewise not observed. (**d**) Three representative curves from panel (a) replotted as conductance $G = 1/R$, vs. temperature, demonstrating the transition into a superinsulating state at finite temperature. The dashed lines show the best fits to Eq. (1) with the corresponding T_{CBKT} listed in the legend. (**e**) Conductance as a function of $(T/T_{CBKT} - 1)^{-1/2}$ for two magnetic fields. The dashed black line is a guide to the eye revealing that linear slopes of the two curves are the same.

simply to a successive deviation from the universal curve: the higher the magnetic field at which the curve is measured, the higher the T/T_{CBKT} ratio at which the given curve departs from the universal envelope. We stress that the above normalization procedure does not presume any special temperature dependence of $G(T)$. The choice of the temperature at which the normalizing value of the conductance is taken is somewhat arbitrary, as seen from the quality of the collapse over the 2.5–5 range in T/T_{CBKT}.

We now describe the overall $G(T, B)$ behavior using a two dimensional Coulomb gas model[5] that generalizes the Kosterlitz formula (1) by incorporating a self-consistent solution to the effects of electronic screening. The conduction is controlled by the density of free charge carriers, $G \propto n_f$, i.e. the conductance is proportional to the inverse squared mean distance between the carriers. In the critical BKT region, n_f is the 2D density of the unbound charges, which is related to the correlation length λ at which the unbound charges appear via the equation:

$$n_f = \frac{1}{2\pi}\left(\frac{1}{\lambda^2} - \frac{1}{\lambda_c^2}\right), \tag{2}$$

where λ_c is the smaller of the bare electrostatic screening length of the film, Λ, or the lateral linear dimension of the film. The screening length defines the maximal spatial scale of logarithmic charge interactions in the film, $V(r) \propto \ln(r/\Lambda)$ for $r_0 < r < \Lambda$. Since $r_0 \approx d \ll \Lambda$, the film is effectively 2D with respect to the Coulomb charge interactions over a broad range of length scales.

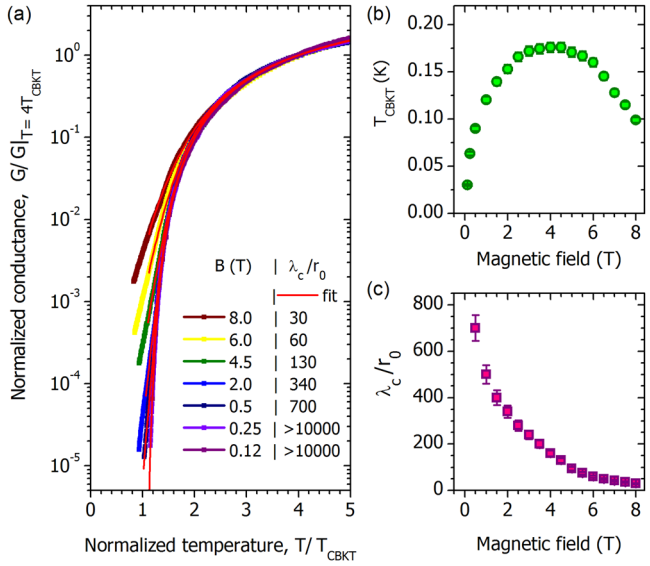

Figure 4. Charge BKT in the 10 nm NbTiN film. (**a**) Normalized conductance vs. normalized temperature. The temperature is normalized with respect to T_{CBKT} and the conductances were normalized by their values at high temperatures, $T = 4T_{CBKT}$. Symbols stand for experimental data, and red lines show the fit obtained from the self-consistent solution to Eqs (2) and (3). We present data covering the full range of magnetic field but omit a few curves to avoid overcrowding the plot. (**b**) Magnetic field dependence of the transition temperatures T_{CBKT}. (**c**) The screening length λ_c in units of r_0 vs. magnetic field.

Relating λ_c and the density of the unbound charges through the Poisson equation, we derive, following[5], a self-consistent equation for λ:

$$\left(\frac{\lambda}{r_0}\right)^{\sqrt{(T/T_{CBKT})-1}} = \mathbb{Z}\cdot\left(1-\frac{\lambda^2}{\lambda_c^2}\right), \tag{3}$$

where $\mathbb{Z}$ is a constant. As $\lambda_c \to \infty$, Eqs (2) and (3), reduce to Eq. (1), with $b = 2\ln(1/\mathbb{Z})$.

We verify this model against the data by fitting a self-consistent solution of Eqs (2) and (3) to the measured isomagnetic G(T) (see representative curves in Fig. 4(a)); the only adjustable parameter in these fits is the screening length λ_c. The field evolution of the derived λ_c values is shown in Fig. 4(c). Thus, we see that the two-dimensional Coulomb gas model fully describes the complex diversity of the experimental data, including both the BKT critical behavior and the deviation from criticality, using only one adjustable parameter.

A signature of the BKT transition is a current-voltage curve of the form $I \propto V^{\alpha}$ at $T \leq T_{BKT}$, with α experiencing a jump from $\alpha = 1$ to $\alpha = 3$ at $T = T_{BKT}$. For our NbTiN films, Fig. 5 displays a set of I–V curves measured as a function of temperature for magnetic field $B = 0.6$ T (I–V curves for additional fields are shown in (See Supplemental Material for further information on the fabrication and measurement techniques, films structural, superconducting and transport parameters, and I–V characteristics)). In this field, the electrostatic screening length is approximately equal to the lateral linear size of the film (see Fig. 4(c)). T_{BKT} determined from $I(V)$ coincides with T_{BKT} determined from $R(T)$.

Discussion and Conclusion

We now discuss the implications of identifying the nature of the Cooper pair insulator as a two-dimensional neutral Coulomb plasma of excessive/deficit Cooper pairs, each carrying the charge $\pm 2e$, and analyze further the parameters of this Cooper pair plasma. We note first the apparent divergence of λ_c upon decreasing B. That λ_c depends on B enables its identification as the electrostatic screening length in disordered films, $\lambda_c = \Lambda = \varepsilon d$. Accordingly, its divergence upon decreasing B corresponds to the divergence of the dielectric constant upon approach to the SIT, with a cutoff of the divergence as λ_c approaches the lateral system size. The value of the magnetic field, $B_{SIT} = 0.015$ T, where the SIT occurs, is determined by the crossing point of the resistive curves, as seen in Fig. 2(b), whose appearance is a hallmark of the field-driven SIT. In the vicinity of the field-driven SIT the corresponding correlation length diverges as $(B - B_{SIT})^{-\tilde{\nu}}$[35], as do the relevant physical quantities. To analyze the character of the divergence we plot λ_c/r_0 vs $(B - B_{SIT})/B_{SIT}$ (Fig. 6(a)), where we see that at the lowest fields $\lambda_c \propto (B - B_{SIT})^{-\nu}$, with $\nu = 0.51 \pm 0.02$ and $\nu = 2.44 \pm 0.04$ further from the transition. In strongly disordered films, one can expect the SIT to be governed by a percolation transition (see[11] and references therein), so it is natural to analyze the scaling behavior in the framework of a random JJA or a random inductor-capacitor network (ICN), with the magnetic field moving the system away from the percolation transition at $B = B_{SIT}$. At large field, the screening length λ_c is not large, and hence the electric behavior of the network is dominated by the nodes' capacitances to ground C_0[11,40]. Numerical analysis of the ICN in the vicinity of the transition in the large C_0 limit[46] yields $\nu = 2.52$, in good agreement with our experimental findings. This establishes the percolative

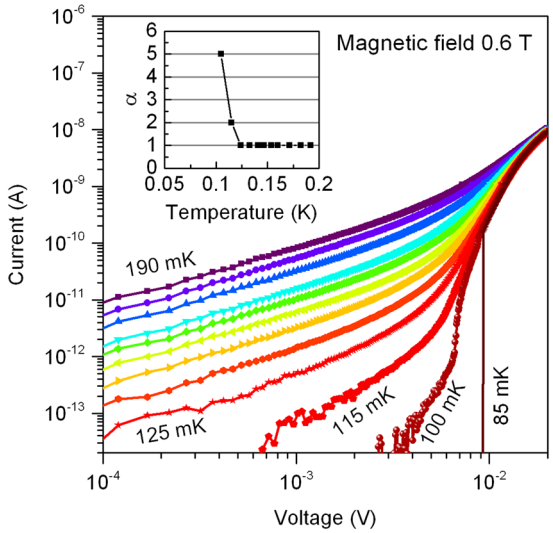

Figure 5. Current-voltage curves in the vicinity of the charge BKT transition. Main panels: Current-voltage curves for a range of temperatures at $B = 0.6$ T. Inset: Onset of superlinear behavior below T_{CBKT}, obtained by fitting the low-current portion of the I-V curves to $I \propto V^{\alpha}$.

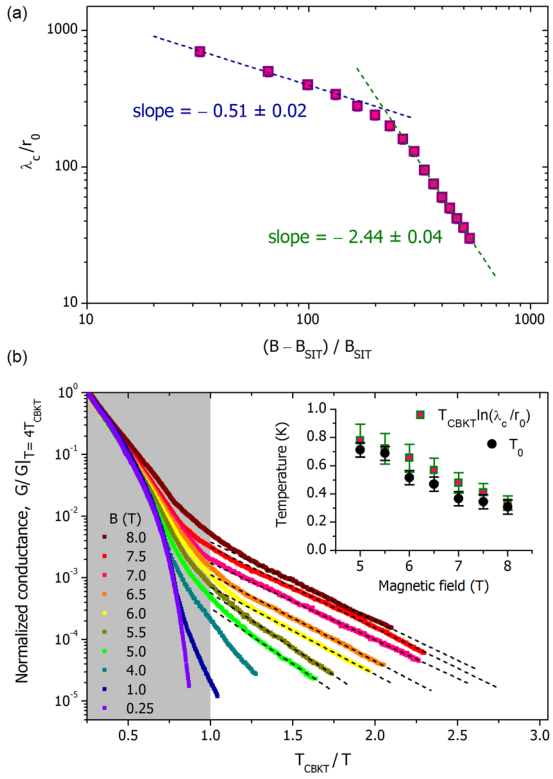

Figure 6. Critical behavior and the effects of the finite electrostatic screening length. (**a**) The screening length λ_c in units of r_0 in a double-log scale as function of $(B - B_{SIT})/B_{SIT}$. At low magnetic fields λ_c follows the power-law dependence shown by the dashed line, $\lambda_c \propto (B - B_{SIT})^{-\nu}$, with $\nu = 0.51 \pm 0.02$. At higher magnetic fields the slope increases and the exponent becomes $\nu' = 2.44 \pm 0.04$. (**b**) Normalized Arrhenius plots of conductances at various fields. The shaded area corresponds to the critical region above T_{CBKT} described by Eqs (2) and (3). The tails at $T < T_{CBKT}$ demonstrate thermally activated behavior highlighted by the dashed lines. The slopes grow with decreasing magnetic field, the corresponding values T_0 of the activation temperature are shown in the inset as black circles. The inset presents a comparison of the activation energies, T_0, and $T_{CBKT} \ln(\lambda_c/r_0)$ shown by squares, evidencing the logarithmic dependence of the activation energy on the screening length, as expected for the 2D logarithmic Coulomb interaction between the charges.

behavior near the transition and suggests that the magnetic field indeed acts as the parameter destroying the superconducting bonds on approach to the SIT from the superconducting side. We thus expect that the superfluid density should scale as $\rho_s \propto (B_{SIT} - B)^{\nu}$. In the limit of $C_0 \to 0$, i.e. in the region of large λ_c[40], the duality principle[11,35,36] implies that on the insulating side the dielectric constant scales as $\varepsilon \sim \rho_s^{-1}$. The exponent $\nu = 0.53$ in the dual limit was found in[47], in agreement with our experimental result of $\nu = 0.51 \pm 0.02$.

Our finding is in a full accord with the polarization catastrophe paradigm built on the divergence of ε as function of the carrier concentration at the approach to the quantum metal-insulator transition[48,49]. In our experiment, it is $B - B_{SIT}$ that plays the role of the deviation of the carrier concentration from its critical value.

Having determined the screening length and T_{CBKT} as a function of magnetic field, we now can make an independent cross-check on the 2D Coulomb nature of the superinsulator. Shown in Fig. 6(b) are Arrhenius plots of the normalized conductance vs. T_{CBKT}/T at various magnetic fields, highlighting the thermally activated behavior at low temperatures, $T < T_{CBKT}$. Note that Eqs (2) and (3) describe conductance only at $T > T_{CBKT}$, shown as a shaded rectangle. The field dependent activation temperatures T_0 are presented in the inset to Fig. 6(b). When the typical size of the unbound pair becomes comparable to Λ, the interaction ceases to be logarithmic and the conductance is dominated by thermodynamically activated free charges. The onset of this activated behavior marks the point at which the correlation length becomes comparable to the screening length. Thus, the low-temperature tails in $G(T)$ are expected to be exponential and to depart from the BKT criticality curve. Theoretical calculations[10,40] and simulations[50] of thermally activated hopping transport in a 2D insulator with logarithmic Coulomb interactions between the charge carriers yield an activation temperature $T_0 \simeq T_{CBKT} \ln(\lambda_c/r_0)$. In the same inset we present our experimental values of $T_{CBKT} \ln(\lambda_c/r_0)$ at the same fields; these indeed appear remarkably close to the independently determined T_0 in accord with the theoretical expectations. This correspondence validates the 2D Coulomb logarithmic interaction between charges at distances not exceeding the screening length. Similarly, exponential low-temperature tails in the resistance were observed in JJA on the superconducting side of the SIT. The tails appeared below the vortex BKT transition temperature where the applied magnetic field introduced the excess unbound vortices[51].

We now can resolve the long-standing open question in the study of the SIT: the origin of the giant peak in the magnetoresistance[17,19,52–54]. It arises from the combination of the dielectric constant rapidly decaying with the increase of the magnetic field and the nonmonotonic behavior of T_{CBKT}. In order to gain insight into the behavior of the latter, we employ the model of JJA, an array of superconducting granules connected with Josephson links, which is a long-standing model for a critically disordered superconducting film[55]. In the parent compound NbN, for example, disordered films were seen to have a self-induced granular structure with the elemental cell having characteristic size ~1–2ξ[56]. It also should be noted that the relevant disorder is electronic rather than structural, and can emerge from structurally homogenous films, particularly when in close proximity to a SIT[57]. The origin of the nonmonotonic behavior of T_{CBKT} can be explained by recalling that the energy gap of the Cooper pair insulator in JJA, $\Delta_c(B)$, is suppressed by the Josephson coupling E_J between the neighboring granules, $\Delta_c(B) = \Delta_c(0)[1 - AE_J(B)/E_c]$[40], where E_c is the Coulomb energy of a single granule and A is a constant. The Josephson coupling is maximal at zero field and, in the irregular JJA, has the minimum at the frustration factor $f = 1/2$[58], where $f \equiv BS/\Phi_0$, S is the average area of the JJA elemental cell and Φ_0 is the magnetic flux quantum. Accordingly, the effective Coulomb energy acquires the *maximum* at $f = 1/2$, i.e. the nonmonotonic behavior of T_{CBKT} reflects the nonmonotonic behavior of E_J as a function of the magnetic field. The non-monotonic nature of E_J also can be directly observed in I–V curves, where the activation voltage varies non-monotonically with field (see SI). This enables us to estimate the parameters of the system as follows. The observed maximum in T_{CBKT} at $B \approx 4$ T (Fig. 4(b)) implies that the average area of an elemental cell of our self-induced granular structure, $S \approx 260\,\text{nm}^2$ and, hence, the linear size of the elemental cell $\sqrt{S} \approx 16\,\text{nm} \approx 3.5\xi$, where $\xi = 4.5$ nm is the superconducting coherence length of the NbTiN film (see SI). Interestingly, this correlates with the analogous estimates for TiN, where $\sqrt{S} \approx 4\xi$ was observed[59]. The described nonmonotonic behavior is accompanied by the overall suppression of the superconducting gap by the increasing magnetic field. The latter eventually would suppress the superconducting gap in Cooper pair droplets and hence Δ_c, resulting in a further drop of the resistance. Then, the Cooper pair insulator ends up as a metal[38].

By comparison to NbTiN, the behaviors complying with the formation of the superinsulating state were observed in other materials at very low temperatures. In TiN films the superinsulator appeared at 40 mK[24]. More recently, the finite temperature zero-conductance state in InO_x was reported at $T \lesssim 35$ mK[19]. The temperature dependence of the conductance in InO_x was found to follow the so-called Vogel-Fulcher-Tamman dependence, $\sigma \propto \exp[-\text{const}/(T^* - T)]$[60–62]. This, however, can be viewed as a manifestation of the same BKT physics, but in a more disordered system[63].

The Kosterlitz-like exponential behavior described by Eq. (1) also appears in the framework of many-body localization (MBL) theory[64,65]. One can thus ask if the observed critical behavior of the NbTiN films should instead be considered in the context of MBL. A detailed comparison of BKT and MBL physics is given in[63], but we briefly note that our data and analysis unambiguously evidences the primary role of the long range two dimensional logarithmic Coulomb interactions between charges which are a platform for BKT physics. By contrast, the original MBL model[64,65] was constructed for one dimensional systems in the strict absence of the long range interactions. While recent work has proposed the extension of MBL to a model with long range interactions[66], it is not clear whether the exponential critical behavior would survive in the systems with interactions. Even more important is that in the MBL framework, taking the system deeper into the insulator (i.e. moving away from the SIT) via increasing magnetic field and/or disorder is expected to enhance localization and hence critical behavior. As discussed above, we observe the opposite trend: increasing magnetic field shrinks the screening length and narrows the window in which the criticality is seen, consistent with the expectations of a BKT system. In sum, this

indicates that at present MBL does not offer the appropriate framework for describing the superinsulating state and its related criticality.

To summarize, our findings clearly establish the finite temperature superinsulating state in NbTiN as the low temperature charge BKT phase of the Cooper pair insulator. We demonstrate superinsulating behavior in a new material with a substantially higher transition temperature of nearly 200 mK, allowing for the first time a detailed characterization of behavior of the system both above and below T_{CBKT} and its evolution in a wide range of magnetic fields.

Methods

The fabrication is built upon the Atomic Layer Deposition technique. The structure of films grown on Si substrates with AlN buffer layers was investigated using a JEOL-4000EX electron microscope operated at 400 kV, with a point-to-point resolution of 0.16 nm and a line resolution of 0.1 nm. The details of sample fabrication, analysis and measurements are given in SM.

Data availability. The authors declare that all relevant data supporting the findings of this study are available within the article and its supplementary information file.

References

1. Berezinskii, V. L. Destruction of long-range order in one-dimensional and two-dimensional systems having a continuous symmetry group I. Classical systems. *Sov. Phys. JETP* **32**, 493 (1970).
2. Kosterlitz, J. M. & Thouless, D. J. Long range order and metastability in two dimensional solids and superfluids. (Application of dislocation theory). *J. Phys. C: Solid State Phys.* **5**, L124 (1972).
3. Kosterlitz, J. M. & Thouless, D. J. Ordering, metastability and phase transitions in two-dimensional systems. *J. Phys. C: Solid State Phys.* **6**, 1181 (1973).
4. Mooij, J. E. In Percolation, Localization and Superconductivity. eds Goldman, A. M. & Wolf, S. A. (Plenum Press, New York and London) 325 (1984).
5. Minnhagen, P. The two-dimensional Coulomb gas, vortex unbinding, and superfluid-superconducting films. *Rev. Mod. Phys.* **59**, 1001 (1987).
6. Fazio, R. & Schön, G. Charge and vortex dynamics in arrays of tunnel junctions. *Phys. Rev. B* **43**, 5307 (1991).
7. Mooij, J. E. *et al*. Unbinding of Charge-Anticharge Pairs in Two-Dimensional Arrays of Small Tunnel Junctions. *Phys. Rev. Lett.* **65**, 638 (1990).
8. Goldman, A. M. The Berezinskii-Kosterlitz-Thouless Transition in Superconducors. In *40 years of the Berezinskii-Kosterlitz-Thouless theory*, 135 World Scientific (2013).
9. Diamantini, M. C., Sodano, P. & Trugenberger, C. A. Gauge theories of Josephson junction arrays. *Nuclear Physics B* **474**, 641 (1996).
10. Vinokur, V. M. *et al*. Superinsulator and quantum synchronization. *Nature* **452**, 316 (2008).
11. Baturina, T. I. & Vinokur, V. M. Superinsulator-superconductor duality in two dimensions. *Annals of Physics* **331**, 236 (2013).
12. Anderson, P. W. Lectures on amorphous systems. III condensed matter in *Les Houches Lectures* North-Holland (1979).
13. Bell, M. T., Sadovskyy, I. A., Ioffe, L. B., Kitaev, A. Yu & Gershenson, M. E. Quantum Superinductor with Tunable Nonlinearity. *Phys. Rev. Lett.* **109**, 137003 (2012).
14. Kowal, D. & Ovadyahu, Z. Disorder induced granularity in an amorphous superconductor. *Solid State Comm.* **90**, 783 (1994).
15. Sambandamurthy, G., Engel, L. M., Johansson, A., Peled, E. & Shahar, D. Experimental evidence for a collective insulating state in two-dimensional superconductors. *Phys. Rev. Lett.* **94**, 017003 (2005).
16. Steiner, M. & Kapitulnik, A. Superconductivity in the insulating phase above the field-tuned superconductor-insulator transition in disordered indium oxide films. *Physica C* **422**, 16 (2005).
17. Baturina, T. I., Mironov, A. Yu, Vinokur, V. M., Baklanov, M. R. & Strunk, C. Localized superconductivity in the quantum-critical region of the disorder-driven superconductor-insulator transition in TiN thin films. *Phys. Rev. Lett.* **99**, 257003 (2007).
18. Baturina, T. I., Mironov, A., Yu., Vinokur, V. M., Baklanov, M. R. & Strunk, C. Hyperactivated Resistance in TiN Films on the Insulating Side of the Disorder-Driven Superconductor-Insulator Transition. *JETP Lett.* **88**, 752 (2008).
19. Ovadia, M. *et al*. Evidence for a finite-temperature insulator. *Sci. Rep.* **5**, 13503 (2015).
20. Kanda, A. & Kobayashi, S. Precursor of Charge KTB Transition in Normal and Superconducting Tunnel Junction Array. *J. Phys. Soc. Japan* **64**, 19 (1995).
21. Kobayashi, S., Kanda, A. & Yamada, R. Charge Kosterlitz-Thouless transition in two-dimensional arrays of small tunnel junctions. *Jpn. J. Appl. Phys.* **34**, 4548 (1995).
22. Kanda, A. & Kobayashi, S. Effect of self-capacitance on charge Kosterlitz-Thouless transition in two-dimensional arrays of small tunnel junctions. *Physica C* **227**, 238 (1996).
23. Baturina, T. I. *et al*. Nanopattern-stimulated superconductor-insulator transition in thin TiN films. *Europhys. Lett.* **93**, 47002 (2011).
24. Kalok, D. *et al*. Non-linear conduction in the critical region of the superconductor-insulator transition in TiN thin films. *J. Phys: Conf. Ser.* **400**, 022042 (2012).
25. Lim, B. S., Rahtu, A. & Gordon, R. G. Atomic layer deposition of transition metals. *Nature Materials* **2**, 749 (2003).
26. Driessen, E. F. C., Coumou, P. C. J. J., Tromp, R. R., de Visser, P. J. & Klapwijk, T. M. Strongly Disordered TiN and NbTiN s-Wave Superconductors Probed by Microwave Electrodynamics. *Phys. Rev. Lett.* **109**, 107003 (2012).
27. Makise, K., Terai, H., Tominari, Y., Tanaka, S. & Shinozaki, B. Duality picture of Superconductor-insulator transitions on Superconducting nanowire. *Sci. Rep.* **6**, 27001 (2016).
28. Proslier, T., Klug, J. A., Becker, N. C., Elam, J. W. & Pellin, M. J. Atomic Layer Deposition of Superconductors. *ECS Transactions* **41**, 237 (2011).
29. Shiino, T. *et al*. Improvement of the critical temperature of superconducting NbTiN and NbN thin films using the AlN buffer layer. *Supercond. Sci. Technol.* **23**, 045004 (2010).
30. Larkin, A. & Varlamov, A. *Theory of Fluctuations in Superconductors*. (Clarendon Press, Oxford, 2005).
31. Berezinskii, V. L. Destruction of Long-range Order in One-dimensional and Two-dimensional Systems Possessing a Continuous Symmetry Group. II. Quantum Systems. *Sov. Phys. JETP* **34**, 1144 (1972).
32. Sacepe, B. *et al*. Disorder-Induced Inhomogeneities of the Superconducting State Close to the Superconductor-Insulator Transition. *Phys. Rev. Lett.* **101**, 157006 (2008).
33. Baturina, T. I. *et al*. Superconducting phase transitions in ultrathin TiN films. *Europhys. Lett.* **97**, 17012 (2012).
34. Chand, M. *et al*. Phase diagram of the strongly disordered s-wave superconductor NbN close to the metal-insulator transition. *Phys. Rev. B* **85**, 014508 (2012).
35. Fisher, M. P. A. Quantum Phase Transitions in Disordered Two-Dimensional Superconductors. *Phys. Rev. Lett.* **65**, 923 (1990).

36. Fisher, M. P. A., Grinstein, G. & Girvin, S. M. Presence of quantum diffusion in two dimensions: Universal resistance at the superconductor-insulator transition. *Phys. Rev. Lett.* **64**, 587 (1990).
37. Goldman, A. M. Superconductor-Insulator Transitions. *Int. J. Mod. Phys. B* **24**, 4081 (2010).
38. Baturina, T. I., Strunk, C., Baklanov, M. R. & Satta, A. Quantum Metallicity on the High-Field Side of the Superconductor-Insulator Transition. *Phys. Rev. Lett.* **98**, 127003 (2007).
39. Das, D. & Doniach, S. Existence of a Bose metal at $T = 0$. *Phys. Rev. B* **60**, 1261 (1999).
40. Fistul, M. V., Vinokur, V. M. & Baturina, T. I. Collective Cooper-Pair Transport in the Insulating State of Josephson-Junction Arrays. *Phys. Rev. Lett.* **100**, 086805 (2008).
41. Baturina, T. I., Bentner, J., Strunk, C., Baklanov, M. R. & Satta, A. From quantum corrections to magnetic-field-tuned superconductor-insulator quantum phase transition in TiN film. *Physica B* **359–361**, 500 (2005).
42. Tikhonov, K. S., Schwiete, G. & Finkel'stein, A. M. Fluctuation conductivity in disordered superconducting films. *Phys. Rev. B* **85**, 174527 (2012).
43. Ovadia, M., Kalok, D., Sacepe, B. & Shahar, D. Duality symmetry and its breakdown in the vicinity of the superconductor-insulator transition. *Nat. Phys.* **9**, 415 (2013).
44. Sacepe, B. *et al*. High-field termination of a Cooper-pair insulator. *Phys. Rev. B* **91**, 220508(R) (2015).
45. Kosterlitz, J. M. The critical properties of the two-dimensional xy model. *J. Phys. C: Solid State Phys.* **7**, 1046 (1974).
46. Loh, Y. L. & Karki, P. Dielectric and diamagnetic susceptibilities near percolative superconductor-insulator transitions. *J. Phys.: Condens. Matter* **29**, 425901 (2017).
47. Granato, E. & Kosterlitz, J. M. Superconductor-Insulator Transition and Universal Resistance in Josephson-Junction Arrays in a Magnetic Field. *Phys. Rev. Lett.* **65**, 1267 (1990).
48. Paalanen, M. A., Rosenbaum, T. F., Thomas, G. A. & Bhatt, R. N. Stress tuning of the metal-insulator transition at millikelvin temperatures. *Phys. Rev. Lett.* **48**, 1284 (1982).
49. Bhatt, R. N. Dielectric function near a polarization catastrophe. *Phil. Mag. B* **50**, 189 (1984).
50. Ortuño, M., Somoza, A. M., Vinokur, V. M. & Baturina, T. I. Electronic transport in two-dimensional high dielectric constant nanosystems. *Sci. Rep* **5**, 9667 (2015).
51. van der Zant, H. J., Rijken, H. A. & Mooij, J. H. The Superconducting Transition of 2-D Josephson-Junction Arrays in a Small Perpendicular Magnetic Field. *J. of Low Temp. Phys.* **79**, 289 (1990).
52. Dubi, Y., Meir, Y. & Avishai, Y. Nature of the superconductor-insulator transition in disordered superconductors. *Nature* **449**, 876 (2007).
53. Nguyen, H. Q. *et al*. Observation of Giant Positive Magnetoresistance in a Cooper Pair Insulator. *Phys. Rev. Lett.* **103**, 157001 (2009).
54. Baturina, T. I. *et al*. Quantum-critical region of the disorder-driven superconductor-insulator transition. *Physica C* **468**, 316 (2008).
55. Tinkham, M. *Introduction to Superconductivity*. (McGraw-Hill, New York, 1996).
56. Kamlapure, A. *et al*. Emergence of nanoscale inhomogeneity in the superconducting state of a homogeneously disordered conventional superconductor. *Sci. Rep.* **3**, 2979 (2013).
57. Ganguly, R. *et al*. Magnetic field induced emergent inhomogeneity in a superconducting film with weak and homogeneous disorder. *Phys. Rev. B* **96**, 054509 (2017).
58. Hollen, S. M., Fernandes, G. E., Xu, J. M. & Valles, J. M. Jr. Collapse of the Cooper pair phase coherence length at a superconductor-to-insulator transition. *Phys. Rev. B* **87**, 054512 (2013).
59. Baturina, T. I. *et al*. Dual threshold diode based on the superconductor-to-insulator transition in ultrathin TiN films. *Appl. Phys. Lett.* **102**, 042601 (2013).
60. Vogel, H. The law of the relationship between viscosity of liquids and the temperature. *Physikalische Zeitschrift* **22**, 645 (1921).
61. Fulcher, G. S. Analysis of recent measurements of the viscosity of glasses. *Journal of the American Ceramic Society* **8**, 339 (1925).
62. Tamman, G. & Hesse, W. Die abhängigkeit der viscosität von der temperatur bie unterkühlten flüssigkeiten. *Zeitschrift für Anorganische und Allgemeine Chemie* **156**, 245 (1926).
63. Sankar, S., Vinokur, V. M. & Tripathi, V. Disordered BKT transition and superinsulation. *Phys. Rev B* **97**, 020507 (2018).
64. Gornyi, I. V., Mirlin, A. D. & Polyakov, D. G. Interacting Electrons in Disordered Wires: Anderson Localization and Low-T Transport. *Phys. Rev. Lett.* **95**, 206603 (2005).
65. Basko, D. M., Aleiner, I. L. & Altshuler, B. L. Metal–insulator transition in a weakly interacting many-electron system with localized single-particle states. *Ann. Phys.* **321**, 1126 (2006).
66. Nandkishore, R. M. & Sondhi, S. L. Many-Body Localization with Long-Range Interactions. *Phys. Rev. X* **7**, 041021 (2017).

Acknowledgements

This work was supported by the Ministry of Education and Science of the Russian Federation, by the Grant of the President RF, project No MK-4628.2016.2 (A.Yu.M., S.V.P., M.V.B., and A.K.G.). The high resolution electron microscopy was performed with support of RSF, project No 14-22-00143. The work at Caltech was supported by National Science Foundation Grant No. DMR-1606858 (D.M.S. and T.F.R.). The work at Argonne was supported by the U.S. Department of Energy, Office of Science, Materials Sciences and Engineering Division (V.M.V., T.P., and visits of T.I.B.). T.I.B. also acknowledges support by the Alexander von Humboldt Foundation and from the Consejeria de Educacian, Cultura y Deporte (Comunidad de Madrid) through the talent attraction program, Ref. 2016-T3/IND-1839. A.Yu.M. and T.I.B. were also supported from the Argonne-University of Chicago collaborative seed grant. We are delighted to thank E. Shimshoni for illuminating discusions.

Author Contributions

T.I.B., V.M.V., and T.F.R. conceived the project and initiated this work; the films were synthesized by T.P.; A.Yu.M., D.M.S., S.V.P., M.V.B., and T.I.B. carried out the experiments; A.K.G. performed high resolution electron microscopy; A.Yu.M., D.M.S., T.F.R., V.M.V., and T.I.B. analyzed the data. All authors discussed the results and contributed in writing the manuscript.

Additional Information

Supplementary information accompanies this paper at https://doi.org/10.1038/s41598-018-22451-1.

Competing Interests: The authors declare no competing interests.

Publisher's note: Springer Nature remains neutral with regard to jurisdictional claims in published maps and institutional affiliations.